

The influence of crystalline electric field on the magnetic properties of CeCd_3X_3 ($X = \text{P}$ and As)

Obinna P. Uzoh¹, Suyoung Kim¹, and Eundeok Mun^{1,2}

¹ Department of Physics, Simon Fraser University,
8888 University Drive, Burnaby, B.C. Canada and

² Center for Quantum Materials and Superconductivity (CQMS),
Sungkyunkwan University, Suwon 16419, South Korea

CeCd_3P_3 and CeCd_3As_3 compounds adopt the hexagonal ScAl_3C_3 -type structure, where magnetic Ce ions on a triangular lattice order antiferromagnetically below $T_N \sim 0.42$ K. Their crystalline electric field (CEF) level scheme has been determined by fitting magnetic susceptibility curves, magnetization isotherms, and Schottky anomalies in specific heat. The calculated results, incorporating the CEF excitation, Zeeman splitting, and molecular field, are in good agreement with the experimental data. The CEF model, with Ce^{3+} ions in a trigonal symmetry, explains the strong easy-plane magnetic anisotropy that has been observed in this family of materials. A detailed examination of the CEF parameters suggests that the fourth order CEF parameter B_4^3 is responsible for the strong CEF induced magnetocrystalline anisotropy, with a large ab -plane moment and a small c -axis moment. The reliability of our CEF analysis is assessed by comparing the current study with earlier reports of CeCd_3As_3 . For both CeCd_3X_3 ($X = \text{P}$ and As) compounds, less than 40 % of $R \ln(2)$ magnetic entropy is recovered by T_N and full $R \ln(2)$ entropy is achieved at the Weiss temperature θ_p . Although the observed magnetic entropy is reminiscent of delocalized $4f$ -electron magnetism with significant Kondo screening, the electrical resistivity of these compounds follows a typical metallic behavior. Measurements of thermoelectric power further validate the absence of Kondo contribution in CeCd_3X_3 .

I. INTRODUCTION

Several f -electron materials with triangular lattices (TL) have shown rich phenomena, where the spin-orbit coupling enhances quantum fluctuations due to the highly anisotropic interactions between $4f$ moments [1–6]. For example, a spin liquid state has been proposed in insulating YbMgGaO_4 [7–11] and NaYbS_2 [12, 13]. The low carrier density system YbAl_3C_3 shows a gap in the magnetic excitation spectrum due to the dimerization of the f electrons in Yb^{3+} pairs [14–17]. Of interest is the easy-plane antiferromagnets CeCd_3X_3 ($X = \text{P}$ and As), a new class of TL system, with a low antiferromagnetic ordering temperature and extremely low carrier density [18–22].

The family of compounds CeM_3X_3 ($M = \text{Al}, \text{Cd}$, and Zn , $X = \text{C}, \text{P}$, and As) have been investigated for their robust ground state properties arising from the interplay between crystalline electric field (CEF) and magnetic exchange interaction on the triangular lattice [16, 18–24]. CeCd_3X_3 materials adopt the hexagonal ScAl_3C_3 -type structure (space group $P6_3/mmc$) with the magnetic Ce^{3+} ions having a trigonal (D_{3d}) point symmetry as shown in Fig. 1(c) [20–23]. In this crystal structure, the Ce layers are well separated by the Cd and X atoms, forming a layered 2D TL in the ab -plane, as depicted in Figs. 1(a) and (b) [20–23]. Thermodynamic and transport property measurements have characterized CeCd_3X_3 as a low carrier density system, with a strong easy plane magnetic anisotropy and antiferromagnetic ordering below $T_N \sim 0.42$ K [19, 22]. The low carrier density means there are insufficient charge carriers to screen all local moments and to mediate Ruderman-

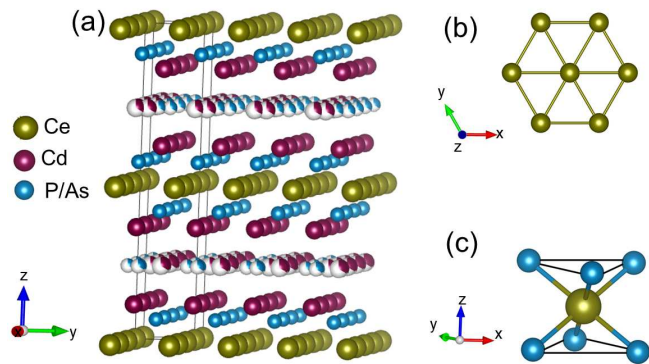


FIG. 1. (a) Crystal structure of the hexagonal CeCd_3X_3 ($X = \text{P}$ and As). (b) Ce atoms forming two-dimensional triangular lattices. (c) Ce atom in a trigonal (D_{3d}) point symmetry surrounded by P/As atoms.

Kittel-Kasuya-Yosida (RKKY) exchange interaction between moments. In this regard, both RKKY and Kondo interactions are expected to be weakened in these compounds. We note that the electrical resistivity measurement on CeCd_3As_3 grown by chemical vapor transport shows a semiconductor-like enhancement as decreasing temperature [20], while the flux grown CeCd_3As_3 sample is metallic [19]. At the magnetic ordering temperature, roughly 40% of $R \ln(2)$ entropy is recovered. This implies a doublet ground state resulting from CEF splitting of localized Ce ion energy levels. The highly enhanced specific heat below 10 K and the reduced magnetic entropy at T_N are reminiscent of Kondo lattice materials. However, the electrical resistivity of CeCd_3X_3 shows no maximum or

TABLE I. CeCd₃As₃: CEF parameters, energy eigenvalues, eigenstates, and molecular field parameters.

CEF and molecular field parameters						
B_2^0 (K)	B_4^0 (K)	B_4^3 (K)	λ_i (mole/emu)			
18.55	-0.08	23.02	$\lambda_{ab} = -5.7,$			
			$\lambda_c = 1.0$			
Energy eigenvalues and eigenstates						
E (K)	$ \frac{-3}{2}\rangle$	$ \frac{-3}{2}\rangle$	$ \frac{-1}{2}\rangle$	$ \frac{1}{2}\rangle$	$ \frac{3}{2}\rangle$	$ \frac{5}{2}\rangle$
0	0.0	0.0	-0.898	0.0	0.0	0.440
0	0.440	0.0	0.0	0.898	0.0	0.0
242	0.0	-1.0	0.0	0.0	0.0	0.0
242	0.0	0.0	0.0	0.0	-1.0	0.0
553	-0.898	0.0	0.0	0.440	0.0	0.0
553	0.0	0.0	0.440	0.0	0.0	0.898

logarithmic upturns resulting from the Kondo scattering of conduction electrons from magnetic Ce ions. The resistivity of CeCd₃X₃ is the same as that of LaCd₃X₃, implying an absence of Kondo screening in these materials [19, 22].

Here, we use the CEF scheme to clarify the anisotropic magnetic properties of CeCd₃X₃ ($X = \text{P}$ and As), where the CEF analysis is performed using the *PyCrystalField* package [26]. For CeCd₃As₃, the CEF analyses of two previous independent studies [20, 25], carried out only considering magnetic susceptibility and magnetization, have shown discrepancies in their energy level splittings and first excited state wave functions. Thus, we extend the CEF analysis to specific heat data to resolve these discrepancies. In contrast to CeCd₃As₃, no CEF analysis has been carried out for CeCd₃P₃. We show that the easy plane magnetic anisotropy observed in these compounds can be explained by the strong CEF acting on Ce³⁺ ions. In addition, we provide evidence of the lacking Kondo screening in these materials by way of thermoelectric power measurements.

II. EXPERIMENTAL

For this work, single crystals of LaCd₃X₃ and CeCd₃X₃ ($X = \text{P}$ and As) were grown by high temperature ternary melt [19, 22, 27]. Magnetization measurements as a function of temperature and magnetic field were performed in a QD MPMS. Specific heat of these compounds was measured in QD PPMS. The obtained results are consistent with earlier reports [19, 22]. Thermoelectric power measurements were performed in a home made two thermometer and one heater setup. Detailed studies of thermodynamic and transport properties of these compounds are presented in Ref. [19, 22].

III. RESULTS & DISCUSSION

For CeCd₃X₃ systems, Ce atoms occupy a single site at the 2*a* Wyckoff position that has a trigonal point sym-

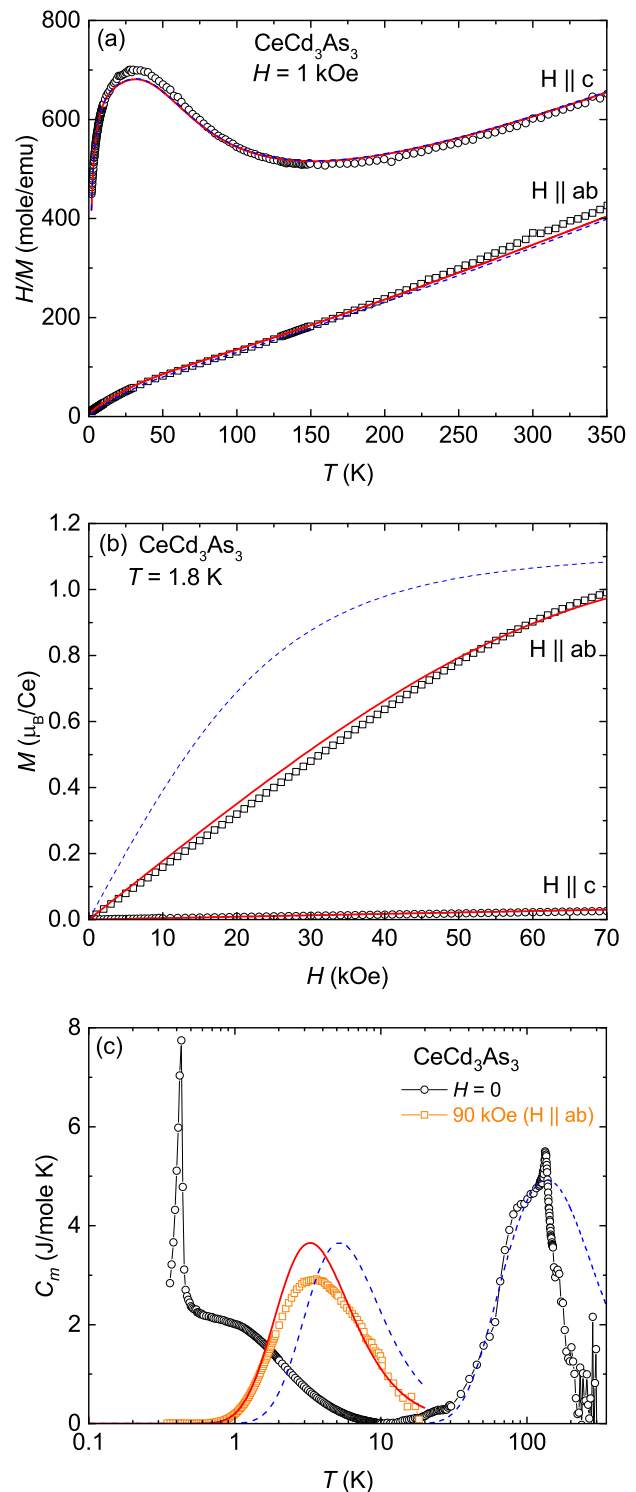


FIG. 2. (a) Inverse magnetic susceptibility curves of CeCd₃As₃, taken at $H = 1$ kOe for both $H \parallel ab$ and $H \parallel c$. (b) Magnetization isotherms at 1.8 K for both $H \parallel ab$ and $H \parallel c$. (c) Magnetic part of the specific heat at $H = 0$ and 90 kOe along $H \parallel ab$. Open symbols are experimental data. Dashed lines represent CEF fits with no molecular field contribution. Solid lines are CEF fits with molecular field terms $\lambda_{ab} = -5.7$ mole/emu and $\lambda_c = 1.0$ mole/emu.

metry, shown in Fig. 1(c). In this point symmetry, the CEF Hamiltonian requires only three parameters [28, 29]: $\mathcal{H}_{CEF} = B_2^0 O_2^0 + B_4^0 O_4^0 + B_4^3 O_4^3$, where O_n^m are the Stevens operators and B_n^m are known as the CEF parameters [30, 31]. It has to be noted here that thermodynamic and transport property measurements of these compounds indicate a possible structural phase transition below 132 K [16, 19, 22]. Additional CEF parameters below the transition temperature are probably required to account for the change in the local environment of the Ce atoms. However, the magnetic susceptibility curves show a smooth evolution through the transition temperature. Therefore, we assume in our CEF analysis that the Ce ions have the same trigonal symmetry below the transition temperature. To account for the Zeeman effect and the interaction between magnetic ions, the eigenvalues and eigenfunctions are determined by diagonalizing the total Hamiltonian: $\mathcal{H} = \mathcal{H}_{CEF} - g_J \mu_B J_i (H_i + \lambda_i M_i)$ ($i = x, y,$ and z), where g_J is the Landé g -factor, μ_B is the Bohr magneton, H_i is the applied field, J_i is the angular momentum operator, and M_i is the magnetization. The second term is the Zeeman contribution and the third term represents the effective molecular interactions λ_i .

The point charge CEF model assumes that the magnetic ions are well localized with a stable valence state. The valence state of CeCd_3X_3 can be deduced from the effective moment of Ce ions. Figures 2(a) and 3(a) show inverse magnetic susceptibility, $\chi^{-1} = H/M$, curves of CeCd_3As_3 and CeCd_3P_3 , respectively. At sufficiently high temperatures, magnetic susceptibility curves follow the Curie-Weiss (CW) behavior: $\chi(T) = C/(T - \theta_p)$, where C is the Curie constant and θ_p is the Weiss temperature. The effective moments of CeCd_3P_3 and CeCd_3As_3 are estimated by applying the CW law to the polycrystalline averaged magnetic susceptibility to be $\mu_{eff} = 2.51 \mu_B$ and $\mu_{eff} = 2.54 \mu_B$, respectively; which agree very well with the theoretical value $\mu_{eff} = 2.54 \mu_B$. From the effective moment values, it is reasonable to assume that Ce ions in these compounds are well localized with 3+ valence state. As shown in Ref. [25, 32] the B_2^0 parameter mainly gives a measure of the magnetocrystalline anisotropy and can be expressed in terms of the Weiss temperatures [33–35]. From the Curie-Weiss fit (not shown), anisotropic Weiss temperatures of CeCd_3As_3 are estimated to be $\theta_{ab} \sim 9.3$ K and $\theta_c = -283$ K. For CeCd_3P_3 , $\theta_{ab} = 9.3$ K and $\theta_c = -248$ K are obtained. The obtained θ_p values are consistent with earlier reports [19, 22]. These values are used to estimate the leading CEF parameters: $B_2^0 \sim 30.5$ K for CeCd_3As_3 and $B_2^0 \sim 26.7$ K for CeCd_3P_3 .

Figure 2 displays anisotropic magnetic susceptibility curves, magnetization isotherms, and specific heat of CeCd_3As_3 with the results of CEF analysis. Table I summarizes the obtained CEF parameters, including molecular field parameters, and the energy eigenstates and eigenvalues. The $2J + 1$ degenerate levels for $J = 5/2$ of Ce^{3+} split into three Kramers doublets with energy level splittings $\Delta_1 = 242$ K and $\Delta_2 = 553$ K. The ground state

and second excited state are in a mixture of $|\pm 5/2\rangle$ and $|\mp 1/2\rangle$ states. However, the first excited state is a pure $|\pm 3/2\rangle$ state.

First, we discuss the CEF effects on thermodynamic properties of CeCd_3As_3 without the molecular field contribution. In Fig. 2, blue dashed-lines represent the CEF evaluations with $\lambda_i = 0$. The CEF fit generally agrees with the inverse magnetic susceptibility as the large anisotropy between crystallographic directions is captured. For $H \parallel c$ the broad hump around 25 K is well reproduced. The CEF model aligns very well with the magnetization isotherm, $M(H)$, for $H \parallel c$ at 1.8 K, whereas there is an inconsistency between the CEF calculation and $M(H)$ for $H \parallel ab$, as shown in Fig. 2(b). The magnetic contribution to the specific heat, C_m , at $H = 0$ and 90 kOe is presented in Fig. 2(c), where C_m is estimated by subtracting the specific heat of non-magnetic analog LaCd_3As_3 . In zero field, the broad maximum near 130 K in C_m can be reproduced by the CEF model. Note that the CEF calculation above the maximum cannot capture the experimental data, which is caused by the very large subtraction error as explained in Ref. [19]. Obviously, the sharp rise of C_m below 10 K and the sharp peak at $T_N = 0.42$ K [19] are not captured by the CEF model. At $H = 90$ kOe for $H \parallel ab$, the overall shape of C_m is captured by the CEF model, but the maximum temperature is higher than that of experimental data.

The CEF model without λ_i does not adequately reproduce $M(H)$ and C_m data for $H \parallel ab$. In order to account for this mismatch, the molecular field interactions between Ce^{3+} ions are incorporated. Red solid-lines in Fig. 2 represent the CEF model in the presence of the molecular field terms: $\lambda_{ab} = -5.7$ mole/emu and $\lambda_c = 1$ mole/emu. The magnetic susceptibility curves with λ_i show a slightly better agreement than that with $\lambda_i = 0$. However, as can be clearly seen in Fig. 2(b), the $M(H)$ curve for $H \parallel ab$ is well captured by the combination of the CEF and λ_i . Moreover, although the absolute value of the maximum in C_m at 90 kOe is slightly higher, the position of the maximum temperature is well reproduced by introducing λ_i . These results point to the importance of including the exchange interactions between Ce^{3+} magnetic ions.

Now turning to the CEF analysis for CeCd_3P_3 , following the same procedure applied to CeCd_3As_3 . The isostructural compounds CeCd_3P_3 and CeCd_3As_3 show remarkably similar magnetic properties, implying that their local CEF environments are in close resemblance. Hence, it is expected that the CEF parameters will be quite similar for both compounds, giving rise to very similar CEF energy level splittings and eigenstates. Table II shows a summary of CEF fit results of CeCd_3P_3 . As expected, the obtained CEF parameters, eigenstates, and eigenvalues for CeCd_3P_3 are very similar to those of CeCd_3As_3 (Table I). The positive B_2^0 term indicates that the magnetization lies in easy plane as seen in Fig. 3(b). The large B_4^3 term implies a mixed ground state with $|\pm 5/2\rangle$ and $|\mp 1/2\rangle$, just like the case for CeCd_3As_3 .

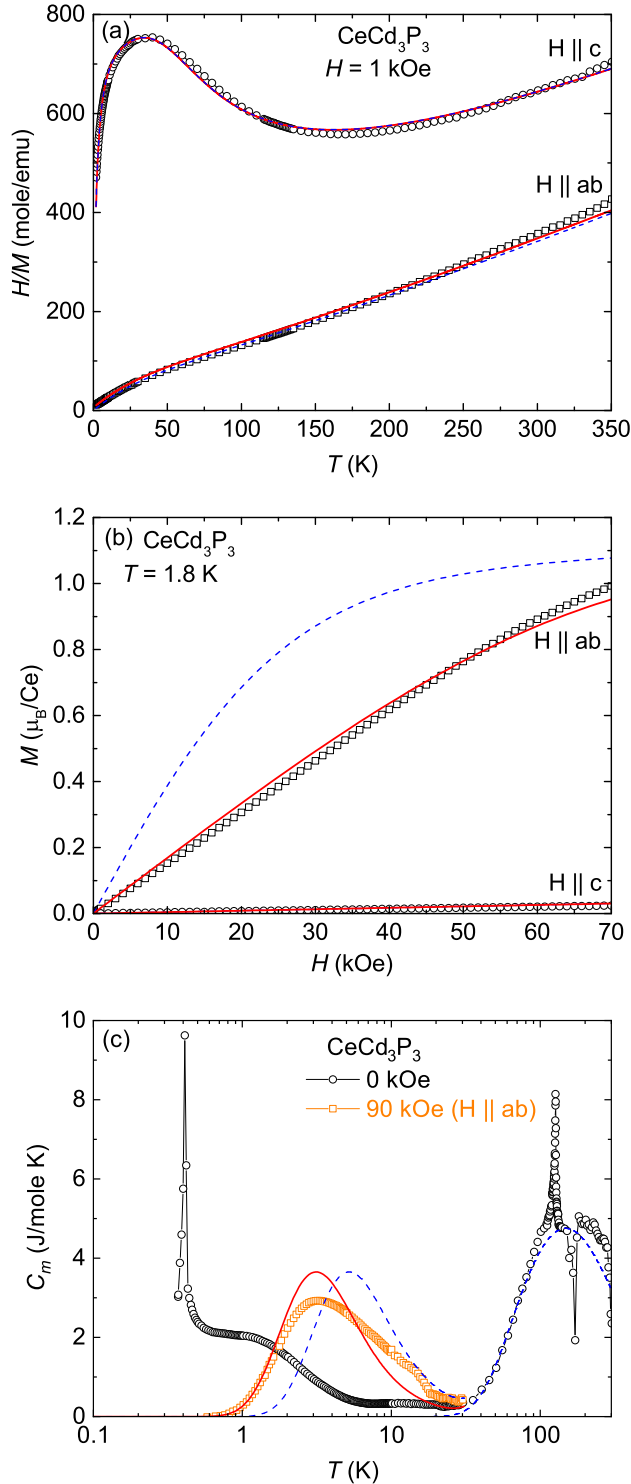


FIG. 3. (a) Inverse magnetic susceptibility curves of CeCd_3P_3 , taken at $H = 1$ kOe for both $H \parallel ab$ and $H \parallel c$. (b) Magnetization isotherms at 1.8 K for both $H \parallel ab$ and $H \parallel c$. (c) Magnetic part of the specific heat at $H = 0$ and 90 kOe along $H \parallel ab$. Open symbols are experimental data. Dashed lines represent CEF fits with no molecular field contribution. Solid lines are CEF fits with molecular field terms $\lambda_{ab} = -6.2$ mole/emu and $\lambda_c = 0.3$ mole/emu.

TABLE II. CeCd_3P_3 : CEF parameters, energy eigenvalues, eigenstates, and molecular field parameters.

CEF and molecular field parameters						
	B_2^0 (K)	B_4^0 (K)	B_4^3 (K)	λ_i (mole/emu)		
	20.90	-0.03	26.00	$\lambda_{ab} = -6.2,$		
				$\lambda_c = 0.3$		
Energy eigenvalues and eigenstates						
E (K)	$ \pm \frac{5}{2}\rangle$	$ \pm \frac{3}{2}\rangle$	$ \pm \frac{1}{2}\rangle$	$ \frac{1}{2}\rangle$	$ \frac{3}{2}\rangle$	$ \frac{5}{2}\rangle$
0	0.0	0.0	-0.897	0.0	0.0	0.442
0	0.442	0.0	0.0	0.897	0.0	0.0
257	0.0	-1.0	0.0	0.0	0.0	0.0
257	0.0	0.0	0.0	0.0	-1.0	0.0
621	-0.897	0.0	0.0	0.442	0.0	0.0
621	0.0	0.0	0.442	0.0	0.0	0.897

The first excited state is in a pure state of $|\pm 3/2\rangle$ and the second excited state is in an admixture of $|\pm 5/2\rangle$ and $|\mp 1/2\rangle$ states. The energy level splittings correspond to 257 K for the first excited state and 621 K for the second excited state.

Figure 3 shows magnetic susceptibility, magnetization, and specific heat curves of CeCd_3P_3 together with the CEF calculations. In the absence of molecular field terms, the CEF calculations (dashed-lines) agree very well with the experimental H/M curves, as shown in Fig. 3(a). Also, in zero field C_m agrees with the CEF fit at high temperatures, as shown in Fig. 3(c), implying the high temperature broad maximum (Schottky anomaly) is due to the CEF effects. The inclusion of the molecular field terms greatly alters the $M(H)$ curve calculation for $H \parallel ab$ and adequately captures the experimental $M(H)$ data. In addition, the CEF calculation with molecular field terms properly captures the low temperature maximum in C_m at $H = 90$ kOe. Therefore, the CEF model in the present of the molecular field interaction should be used to describe the experimental data for CeCd_3P_3 . As expected from the layered crystal structure, the absolute value of λ_{ab} is greater than λ_c , implying a strong exchange interaction in the ab -plane.

The obtained CEF parameters of CeCd_3P_3 are slightly larger than those of CeCd_3As_3 . The slight difference in the values of their CEF parameters is quite surprising. When the distance between Ce and nearest As/P atoms is considered, the difference between Ce-As distance (3.05 Å) and Ce-P distance (2.96 Å) is about ~ 9 pm [19, 20, 22], which might not be large enough to cause different CEF energy level splittings. Note that the validity of the CEF Hamiltonian must be verified below the (structural) phase transition temperature $T_s = 127$ K for CeCd_3P_3 [22] and $T_s = 136$ K for CeCd_3As_3 [19].

In Fig. 4(a) we compare the energy level splittings and eigenfunctions for three independent CEF analyses of CeCd_3As_3 . For all three studies the CEF parameters are obtained from fits to the magnetic susceptibility curves. In this study, the Hamiltonian includes the molecular field term. In Ref. [20] (Study A), the CEF parameters are obtained in the presence of antiferromagnetic

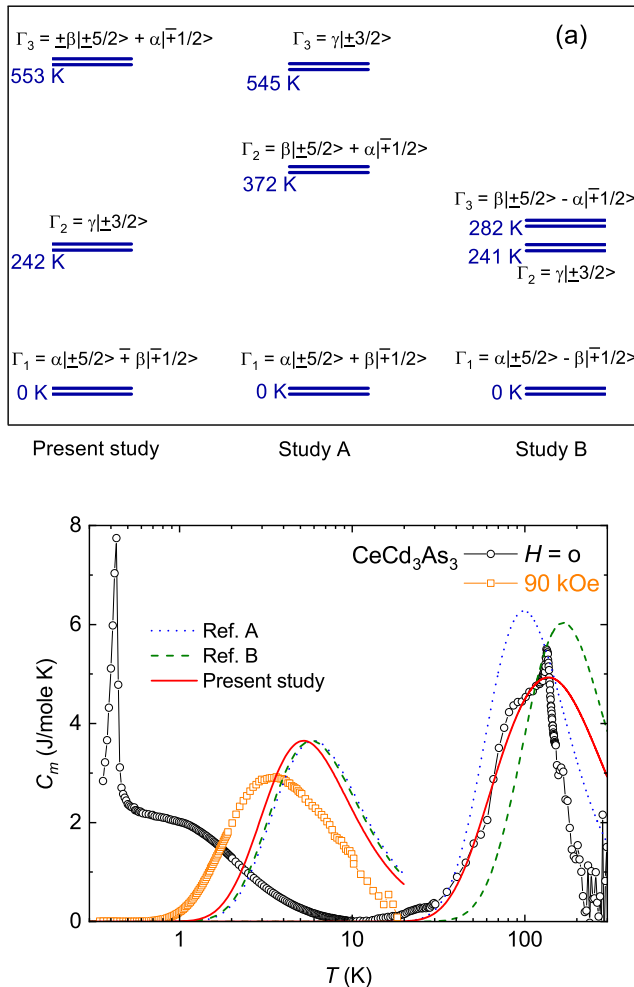


FIG. 4. CEF profiles of CeCd_3As_3 for three independent studies. Study A is from Ref. [20] and Study B is from Ref. [25]. (a) CEF energy level splittings and eigenstates. Present study: $\alpha = 0.44$, $\beta = 0.90$, and $\gamma = -1$. Study A: $\alpha = 0.32$, $\beta = 0.95$, and $\gamma = 1$. Study B: $\alpha = 0.28$, $\beta = 0.96$, and $\gamma = 1$. (b) Comparison between C_m of present study and CEF calculations based on the three independent studies, where $\lambda_i = 0$.

exchange interaction based on a mean-field approach. In Ref. [25] (Study B), the CEF parameters are evaluated by fitting the magnetic susceptibility curves to only \mathcal{H}_{CEF} (without any interaction term).

For all three studies, the ground state (Γ_1) is in a mixed state of $|\pm 5/2\rangle$ and $|\mp 1/2\rangle$ with a higher probability in the $|\mp 1/2\rangle$ state. This requires a mixing angle θ in the wave function: $\cos(\theta)|\pm 5/2\rangle + \sin(\theta)|\mp 1/2\rangle$. The obtained mixing angle is roughly similar for all three studies: 64° in this study, 72° in Ref. [20], and 74° in Ref. [25]. Unlike the ground state, the excited states Γ_2 and Γ_3 do not entirely agree for all three studies. In Ref. [20] there is a clear swap between Γ_2 and Γ_3 wave functions (Study A). This is caused by the relatively high $|B_4^0|$ value ($= 1.4$ K). In fact, we confirmed that any $|B_4^0| > 0.7$ K would

result in the Γ_2 being in a mixed state and the Γ_3 being in a pure state, just as the case in Ref. [20]. Another important distinction among these three studies is in the energy level splittings. The energy eigenvalue for the second excited state in Ref. [25] (Study B) is roughly two times smaller than that of the other two studies. However, the energy level splitting from the ground to the first excited state (~ 240 K) is comparable for all studies, clearly indicating that the ground state is well isolated from the excited states.

Figure 4 (b) shows the magnetic part of the specific heat, together with the calculated specific heat curves by using CEF parameters. Solid lines, dashed lines, and dotted lines are CEF calculations from the present study, Ref. [20], and Ref. [25], respectively. As shown in the figure, when subtle differences are ignored, the high temperature maximum is captured by all three calculated curves. This implies that the high temperature maximum in C_m is due to the CEF effect and the ground state doublet is well isolated from the excited states. When measurement uncertainty and different sample quality are considered, the best CEF parameters among three parameter sets cannot be selected from the comparison with C_m . Therefore, further measurements such as inelastic neutron scattering with Cd isotopes are necessary to distinctly specify the best CEF parameters in this system. In addition, the CEF scheme can be determined by optical spectroscopy techniques such as Raman scattering. Note that CEF parameters evaluated by the three independent studies provide a qualitatively good description of the experimental M/H curves.

The significance of B_4^3 CEF parameter has been observed in Ce-based antiferromagnets such as CeAuSn , CeIr_3Ge_7 , and CeCd_3X_3 , where Ce ions are in a trigonal environment [25, 28, 36]. These compounds indicate a large magnetic anisotropy with the ab -plane being the magnetic easy plane, which can be qualitatively explained by the CEF effect. A detailed CEF analysis based on both the magnetic susceptibility and inelastic neutron scattering data of hexagonal CeAuSn indicates a mixture of $|\pm 5/2\rangle$ and $|\mp 1/2\rangle$ CEF ground state doublet, a pure $|\pm 3/2\rangle$ doublet as the first excited state at ~ 345 K, and a mixture of $|\pm 5/2\rangle$ and $|\mp 1/2\rangle$ doublet as the second excited state at ~ 440 K [28, 36]. The anisotropy ratio of magnetic susceptibility between $H \parallel ab$ and $H \parallel c$ is found to be $\chi_{ab}/\chi_c \sim 15$ near T_N . Both magnetic susceptibility [28] and neutron scattering [36] CEF evaluations clearly show a significant B_4^3 contribution (~ 19 K) with a large mixing angle, which is consistent with the CEF analysis of CeCd_3X_3 . The anisotropy ratio of CeCd_3X_3 ($\chi_{ab}/\chi_c \sim 36$ at 1.8 K) is larger than that of CeAuSn because both B_2^0 and B_4^3 CEF parameters of CeCd_3X_3 are larger than those of CeAuSn . The CEF investigation of the rhombohedral CeIr_3Ge_7 compound shows a very similar CEF eigenstates and eigenvalues with those of other compounds. However, in CeIr_3Ge_7 , the reported CEF parameters (especially the term $B_4^3 = 67.3$ K) are larger than that of other compounds, thus inducing a

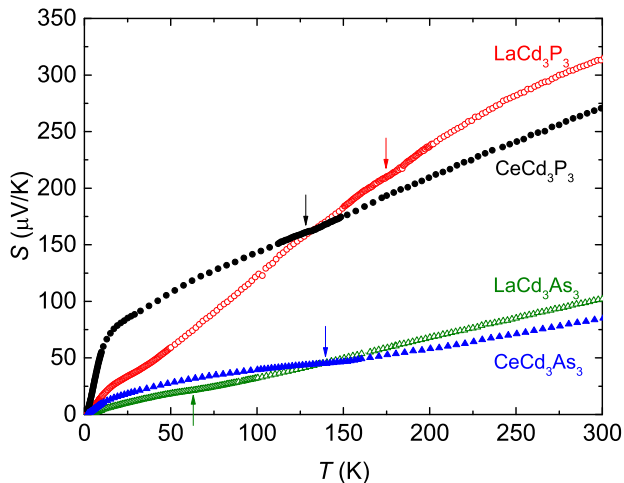


FIG. 5. Temperature dependence of the thermoelectric power, $S(T)$, of RCd_3X_3 ($R = \text{La}$ and Ce , $X = \text{P}$ and As). Vertical arrows indicate the phase transition temperatures observed in electrical resistivity measurements [19, 22].

huge energy level splittings of 374 K and 1398 K. [25]. It has been suggested that the exceptionally large CEF splitting can be related to the contribution of the $5d$ ligands of Ir atoms. [25]. In addition, the CEF analysis on rhombohedral $\text{CePtAl}_4\text{Ge}_2$ antiferromagnet has also been conducted [29]. Unlike the above mentioned compounds, the ground state and the second excited state of $\text{CePtAl}_4\text{Ge}_2$ are not in a mixed configuration of $|5/2\rangle$ and $|1/2\rangle$ states. The sign and magnitude of B_2^0 ($= 13.26$ K) and B_4^0 ($= -0.3$ K) CEF parameters in $\text{CePtAl}_4\text{Ge}_2$ are comparable to that of CeAuSn , CeIr_3Ge_7 , and CeCd_3X_3 ($X = \text{P}$ and As). However, because the B_4^3 term responsible for mixing is exceptionally small in $\text{CePtAl}_4\text{Ge}_2$ system ($B_4^3 = 0 \pm 0.02$ K), the ground state and second excited state is in a pure $|\pm 1/2\rangle$ state and a pure $|\mp 5/2\rangle$ state, respectively. We found that the ground and excited states are without mixing for any $|B_4^3| < 1.1$ K. The small value of B_2^0 and B_4^3 implies a relatively smaller magnetic anisotropy in $\text{CePtAl}_4\text{Ge}_2$, which is clearly reflected on its magnetic susceptibility data ($\chi_{ab}/\chi_c \sim 4$ near T_N) [29].

Although our CEF analysis on CeCd_3X_3 ($X = \text{P}$ and As) provides a comprehensive picture at high temperatures, a number of unanswered questions remains at low temperatures. When the temperature is much lower than the CEF splitting, the lowest Kramers doublet is only relevant to explain the observed magnetic ordering at $T_N = 0.42$ K and upturn in C_m below 10 K. It is obvious that the temperature dependence and absolute value of C_m below 10 K cannot be explained by the CEF effects as shown in Figs. 3(c) and 4(c).

Since magnetization isotherms at $T = 1.8$ K for both compounds are reproduced well by CEF calculation with the ground state wave functions, the reduced magnetization value cannot be associated with the Kondo screen-

ing. This is consistent with the electrical resistivity results of CeCd_3X_3 [19, 22]. The absence of Kondo effect in CeCd_3X_3 is also confirmed from thermoelectric power (TEP) measurements, as shown in Fig. 5. The observed TEP value of LaCd_3X_3 is an order of magnitude higher than that of typical metals, implying low carrier density system. The temperature dependence of the TEP, $S(T)$, of both La- and Ce-based compounds shows a hump at low temperatures, which can be related to the phonon drag. In general, $S(T)$ of typical metals shows a maximum, corresponding to the phonon-drag effect, where the maximum is expected to be located between $\Theta_D/5$ and $\Theta_D/12$ [37]. Many Ce- and Yb-based Kondo lattice systems have shown that $S(T)$ indicates an extrema with enhanced value, corresponding to the Kondo effect in conjunction with CEF effect. The TEP of CeCd_3X_3 exhibits behavior similar to that of LaCd_3X_3 , implying negligible Kondo contributions. Hence, as suggested in Refs. [19, 22], the enhancement of the specific heat below 10 K is likely related to either the magnetic frustration in triangular lattices [18–22] or simply the magnetic fluctuations observed in insulating antiferromagnets [38].

The electrical resistivity of CeCd_3X_3 compounds exhibits a metallic behavior, suggesting that Ruderman-Kittel-Kasuya-Yosida (RKKY) interaction may be responsible for the magnetic ordering. However, it would have to be mediated by an extremely small number of charge carriers [19, 22]. It has been qualitatively shown that the magnetic ordering temperature of non-Kondo materials scale with the distance between Ce ions, where the larger the Ce-Ce distance results in a smaller ordering temperature [39]. For example, a non-Kondo metal CeIr_3Ge_7 orders at an extremely low temperature $T_N = 0.63$ K due to the large Ce-Ce distance (~ 6 Å). When the Ce-Ce distance (~ 4 Å) for CeCd_3X_3 is considered, the magnetic ordering temperature is significantly suppressed compared to that of other Ce-based non-Kondo systems. On the contrary, it has been suggested that the superexchange interaction in low carrier density YbAl_3C_3 compound becomes dominant instead of the RKKY interaction, where the carrier concentration is estimated to be $n \sim 0.01$ per formula unit (f.u.) [14]. When the carrier concentrations of CeCd_3As_3 ($n \sim 0.003/\text{f.u.}$) [19] and CeCd_3P_3 ($n \sim 0.002/\text{f.u.}$) [22] compounds are considered, it is reasonable to assume that the superexchange interaction may be responsible for the antiferromagnetic ordering below 0.42 K. In addition, the partial $H - T$ phase diagram of these compounds, especially the field-induced increase of T_N , is similar to that of 2D insulating triangular lattice systems with easy-plane anisotropy [40, 41]. Furthermore, the low temperature specific heat of CeCd_3As_3 has been explained by anisotropic exchange Hamiltonian for an insulating, layered triangular lattice [20].

IV. CONCLUSION

At high temperatures, the observed magnetic properties of CeCd_3X_3 triangular lattice compounds can be well understood by considering the CEF effects with molecular field contributions. The large anisotropy in the magnetic susceptibility and magnetization and the electronic Schottky anomaly in the specific heat are explained by energy level splittings of the $J = 5/2$ Hund's rule ground state of Ce^{3+} ions into three doublets. The striking similarity of the CEF profile of both compounds implies a very close resemblance of their crystal field environment. Three independent CEF analyses on CeCd_3As_3 indicate inconsistent CEF profiles, requiring further studies such as inelastic neutron scattering. When the temperature is well below the CEF splitting, the well-isolated Kramers' doublet ground state is responsible for the antiferromag-

netic ordering and the large enhancement of specific heat below 10 K. Further measurements such as magnetization, neutron scattering, and nuclear magnetic resonance are necessary to provide additional insight into the nature of magnetism below T_N and the role of anisotropic exchange interactions in the triangular motif.

ACKNOWLEDGMENTS

This work was supported by the Canada Research Chairs, Natural Sciences and Engineering Research Council of Canada, and Canada Foundation for Innovation program. EM was supported by the Korean Ministry of Science and ICT (No. 2021R1A2C2010925) and by BrainLink program funded by the Ministry of Science and ICT (2022H1D3A3A01077468) through the National Research Foundation of Korea.

-
- [1] W.-J. Hu, S.-S. Gong, W. Zhu, and D. N. Sheng, *Phys. Rev. B* **92**, 140403(R) (2015).
- [2] Y.-D. Li, X. Wang, and G. Chen, *Phys. Rev. B* **94**, 035107 (2016).
- [3] Y. Iqbal, W.-J. Hu, R. Thomale, D. Poilblanc, and F. Becca, *Phys. Rev. B* **93**, 144411 (2016).
- [4] S.-S. Gong, W. Zhu, J.-X. Zhu, D. N. Sheng, and K. Yang, *Phys. Rev. B* **96**, 075116 (2017).
- [5] Z. Zhu, P. A. Maksimov, S. R. White, and A. L. Chernyshev, *Phys. Rev. Lett.* **120**, 207203 (2018).
- [6] J. G. Rau and M. J. P. Gingras, *Phys. Rev. B* **98**, 054408 (2018).
- [7] Y. Li, H. Liao, Z. Zhang, S. Li, F. Jin, L. Ling, L. Zhang, Y. Zou, L. Pi, Z. Yang, J. Wang, Z. Wu, and Q. Zhang, *Sci. Rep.* **5**, 16419 (2015).
- [8] Y. Li, G. Chen, W. Tong, L. Pi, J. Liu, Z. Yang, X. Wang, and Q. Zhang, *Phys. Rev. Lett.* **115**, 167203 (2015).
- [9] Y. Shen, Y.-D. Li, H. Wo, Y. Li, S. Shen, B. Pan, Q. Wang, H. Walker, P. Steffens, M. Boehm, Y. Hao, D. L. Quintero-Castro, L. W. Harriger, M. D. Frontzek, L. Hao, S. Meng, Q. Zhang, G. Chen, and J. Zhao, *Nature* **540**, 559 (2016).
- [10] Y. Li, D. Adroja, P. K. Biswas, P. J. Baker, Q. Zhang, J. Liu, A. A. Tsirlin, P. Gegenwart, and Q. Zhang, *Phys. Rev. Lett.* **117**, 097201 (2016).
- [11] J. A. Paddison, M. Daum, Z. Dun, G. Ehlers, Y. Liu, M. B. Stone, H. Zhou, and M. Mourigal, *Nat. Phys.* **13**, 117 (2017).
- [12] M. Baenitz, P. Schlender, J. Sichelschmidt, Y. A. Onykiienko, Z. Zangeneh, K. M. Ranjith, R. Sarkar, L. Hozoi, H. C. Walker, J.-C. Orain, H. Yasuoka, J. van den Brink, H. H. Klauss, D. S. Inosov, and T. Doert, *Phys. Rev. B* **98**, 220409(R) (2018).
- [13] J. Sichelschmidt, P. Schlender, B. Schmidt, M. Baenitz, and T. Doert, *J. Phys.: Condens. Matter* **31**, 205601 (2019).
- [14] A. Ochiai, T. Inukai, T. Matsumura, A. Oyamada, and K. Katoh, *J. Phys. Soc. Jpn.* **76**, 123703 (2007).
- [15] Y. Kato, M. Kosaka, H. Nowatari, Y. Saiga, A. Yamada, T. Kobiyama, S. Katano, K. Ohoyama, H. S. Suzuki, N. Aso, and K. Iwasa, *J. Phys. Soc. Jpn.* **77**, 053701 (2008).
- [16] A. Ochiai, K. Hara, F. Kikuchi, T. Inukai, E. Matsuoka, H. Onodera, S. Nakamura, T. Nojima, and K. Katoh, *J. Phys.: Conf. Ser.* **200**, 022040 (2010).
- [17] K. Hara, S. Matsuda, E. Matsuoka, K. Tanigaki, A. Ochiai, S. Nakamura, T. Nojima, and K. Katoh, *Phys. Rev. B* **85**, 144416 (2012).
- [18] Y. Liu, S. Zhang, J. Lv, S. Su, T. Dong, G. Chen, and N. Wang, arXiv preprint arXiv:1612.03720 (2016).
- [19] S. R. Dunsiger, J. Lee, J. E. Sonier, and E. D. Mun, *Phys. Rev. B* **102**, 064405 (2020).
- [20] K. E. Avers, P. A. Maksimov, P. F. S. Rosa, S. M. Thomas, J. D. Thompson, W. P. Halperin, R. Movshovich, and A. L. Chernyshev, *Phys. Rev. B* **103**, L180406 (2021).
- [21] S. Higuchi, Y. Noshima, N. Shirakawa, M. Tsubota, and J. Kitagawa, *Mater. Res. Express* **3**, 056101 (2016).
- [22] J. Lee, A. Rabus, N. R. Lee-Hone, D. M. Broun, and E. Mun, *Phys. Rev. B* **99**, 245159 (2019).
- [23] S. S. Stoyko and A. Mar, *Inorg. Chem.* **50**, 11152 (2011).
- [24] A. Ochiai, N. Kabeya, K. Maniwa, M. Saito, S. Nakamura, and K. Katoh, *Phys. Rev. B* **104**, 144420 (2021).
- [25] J. Banda, B. K. Rai, H. Rosner, E. Morosan, C. Geibel, and M. Brando, *Phys. Rev. B* **98**, 195120 (2018).
- [26] A. Scheie, *J. Appl. Crystallogr.* **54**, 356 (2021).
- [27] P. C. Canfield and Z. Fisk, *Philos. Mag. B* **65**, 1117 (1992).
- [28] C. L. Huang, V. Fritsch, B. Pilawa, C. C. Yang, M. Merz, and H. v. Löhneysen, *Phys. Rev. B* **91**, 144413 (2015).
- [29] S. Shin, V. Pomjakushin, L. Keller, P. F. S. Rosa, U. Stuhr, C. Niedermayer, R. Sibille, S. Toth, J. Kim, H. Jang, S.-K. Son, H.-O. Lee, T. Shang, M. Medarde, E. D. Bauer, M. Kenzelmann, and T. Park, *Phys. Rev. B* **101**, 224421 (2020).
- [30] K. W. H. Stevens, *Proc. Phys. Soc. A* **65**, 209 (1952).
- [31] M. T. Hutchings, *Solid State Phys.* **16**, 227 (1964).

- [32] C. Klingner, C. Krellner, M. Brando, C. Geibel, and F. Steglich, *New J. Phys.* **13** 083024 (2011).
- [33] Y.-L. Wang, *Physics Letters A* **35**, 383 (1971).
- [34] G. J. Bowden, D. S. P. Bunbury, and M. A. H. McCausland, *J. Phys. C: Solid State Phys.* **4** 1840 (1971).
- [35] N. Shohata, *J. Phys. Soc. Jpn.* **42**, 1873 (1977).
- [36] D. T. Adroja, B. D. Rainford, and A. J. Neville, *J. of Phys.: Condens. Matter* **9**, L391 (1997).
- [37] F. J. Blatt, P. A. Schroeder, C. L. Foiles, and D. Greig, Springer US, Boston, MA (1976).
- [38] W. K. Robinson and S. A. Friedberg, *Phys. Rev.* **117**, 402 (1960).
- [39] Binod K. Rai, Jacintha Banda, Macy Stavinoha, R. Borth, D.-J. Jang, Katherine A. Benavides, D. A. Sokolov, Julia Y. Chan, M. Nicklas, Manuel Brando, C.-L. Huang, and E. Morosan, *Phys. Rev. B* **98**, 195119 (2018).
- [40] L. Seabra, T. Momoi, P. Sindzingre, and N. Shannon, *Phys. Rev. B* **84**, 214418 (2011).
- [41] D. H. Lee, J. D. Joannopoulos, J. W. Negele, and D. P. Landau, *Phys. Rev. B* **33**, 450 (1986).